Spatiotemporal concentration patterns associated with the catalytic oxidation of CO and Au covered Pt(110) surfaces

K. Asakura, J. Lauterbach, H. H. Rotermund, and G. Ertl

Citation: The Journal of Chemical Physics **102**, 8175 (1995); doi: 10.1063/1.469229
View online: http://dx.doi.org/10.1063/1.469229
View Table of Contents: http://scitation.aip.org/content/aip/journal/jcp/102/20?ver=pdfcov
Published by the AIP Publishing

Spatiotemporal concentration patterns associated with the catalytic oxidation of CO and Au covered Pt(110) surfaces

K. Asakura,[a] J. Lauterbach, H. H. Rotermund, and G. Ertl
Fritz-Haber-Institut der Max-Planck-Gesellschaft, Faradayweg 4-6, D-14195 Berlin (Dahlem), Germany

(Received 5 October 1994; accepted 16 February 1995)

Submonolayers of gold were evaporated onto a Pt(110) surface in order to study the influence of surface modification on the formation of spatiotemporal concentration patterns during catalytic oxidation of carbon monoxide as imaged by means of photoemission electron microscopy (PEEM). Already the presence of 0.05 monolayers of uniformly distributed Au atoms affects markedly the kinetic parameters and thereby the properties of spatiotemporal patterns. The excitable regime is reached at lower CO pressures than with bare Pt(110), the width of the oxygen waves and the wavelength of spiral patterns decrease, the velocity of front propagation is reduced, and the density of nucleation centers for waves increases. The observed effects can be rationalized on the basis of the well-established underlying mechanism in terms of modification of the sticking coefficients for oxygen and carbon monoxide and of the diffusion coefficient for adsorbed CO. Additional effects such as penetration of waves into a monostable region, refraction, etc., come into play if waves pass the border between surface areas with differing chemical properties. © *1995 American Institute of Physics.*

I. INTRODUCTION

Chemical reactions in open systems far from equilibrium may give rise to various phenomena of nonlinear dynamics, in particular formation of spatiotemporal concentration patterns.[1,2] Catalytic reactions occurring at well-defined single crystal surfaces are of particular conceptual simplicity in this context because of the reduction of the problem to two dimensions, and have been studied extensively in the past few years.[3,4] Most detailed investigations were performed with the catalytic oxidation of carbon monoxide on a Pt(110) surface[5–9] by applying photoemission electron microscopy (PEEM) as imaging technique.[10] Well-established knowledge on the microscopic mechanism of this reaction enables successful theoretical modeling of the kinetics[11] as well as of spatiotemporal pattern formation.[8,12–14] The latter comprise a variety of phenomena such as propagating wave fronts, spirals, target patterns, and solitary waves, etc., taking place on mesoscopic (i.e.,>10 μm) length scales with characteristic times in the s range. Within the framework of theoretical description in terms of partial differential equations of the reaction-diffusion type, the properties of these patterns are determined by the kinetic parameters of the underlying elementary steps of adsorption, surface diffusion, etc. These quantities depend on the nature of the catalyzing surface, and it was hence of interest to learn how controlled modification of the surface affects the phenomenology of concentration patterns. This goal was achieved by depositing submonolayer quantities of inert Au atoms onto the clean Pt(110) surface. Partial shielding of the sample during the evaporation process enabled, in addition, the preparation of adjacent areas with differing surface composition which were then used to study the effects of boundaries.

Modification of the Pt surface by Au was performed for the following reasons: Au atoms were reported to be homogeneously distributed on a platinum substrate up to completion of a monolayer and bulk diffusion starts only at temperatures above 800 K.[15,16] Their presence causes hence, on the mesoscopic length scale of interest, just a variation of the (averaged) kinetic parameters. Au does not adsorb either oxygen or carbon monoxide above room temperature, but leaves the adsorptive properties of neighboring Pt sites unaffected.[16] In this way just the effective sticking coefficients for CO and O_2 will be reduced (but to different extents, as will be shown). In addition, Au atoms represent obstacles for migrating adsorbed CO molecules, so that also their diffusion coefficient (which is of relevance for the pattern formation) will be diminished.

The present paper contains full account of our experimental findings, for which a brief report has already been given elsewhere.[17]

II. EXPERIMENT

The experiments were carried out in an UHV system with a base pressure below 2×10^{-11} mbar. A gas inlet system with feedback stabilization enabled constant setting of the CO and O_2 partial pressures.[9,18] Imaging of concentration patterns arising from the two adsorbates (CO_{ad} and O_{ad}) was performed by means of a photoemission electron microscope (PEEM)[10] whose contrast is based on local work function variations arising from differing dipole moments of the adsorbate complexes. The spatial resolution of this instrument is about 0.2 μm, while a section of the sample surface with a diameter of up to 700 μm is viewed. Temporal resolution is limited by the frequency of the video tape on which the patterns are stored, i.e., 20 ms. In the images predominantly O-covered regions appear dark, those which are essentially CO-covered are grey.

The Pt(110) samples were prepared by standard procedures consisting of cycles of oxidation at elevated tempera-

[a]Permanent address: Research Center for Spectrochemistry, Faculty of Science, University of Tokyo, Hongo, Bunkyo-ku, Tokyo 113, Japan.

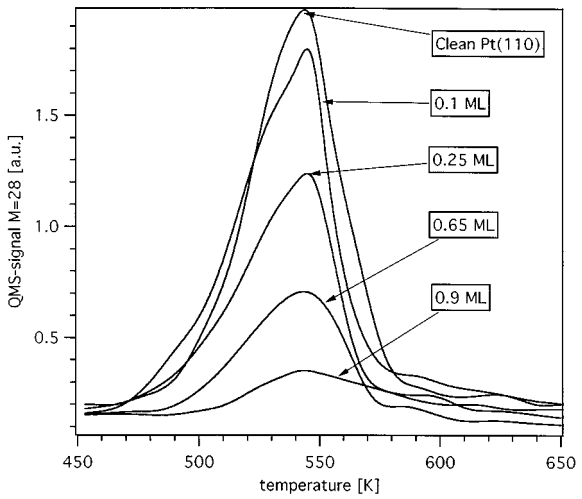

FIG. 1. Thermal desorption spectra for CO from a Pt(110) surface with varying Au concentrations. Heating rate 5 K/s.

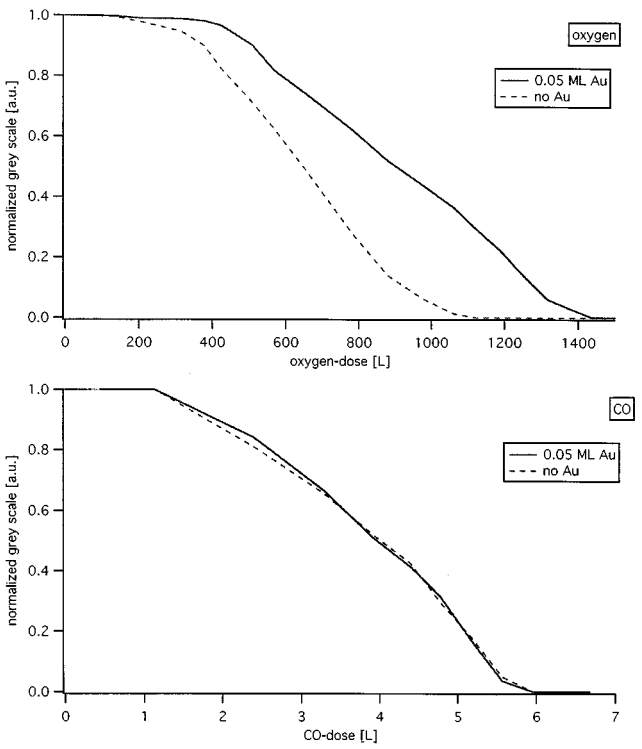

FIG. 2. Variation of the normalized integral intensity of PEEM images from bare Pt(110) (full lines) and a surface precovered with 0.05 ML Au (broken lines) as a function of time upon exposure to 2×10^{-7} mbar CO (a) and 6×10^{-5} mbar O_2 (b), respectively.

tures, noble gas ion sputtering and annealing up to 1100 K. Au films were evaporated onto the clean Pt(110) surface from a resistively heated Au-covered tungsten filament. The rate of deposition was monitored by an oscillating quartz microbalance (Leybold XTC/2). Determination of the absolute gold coverage was achieved by CO titration as described below. Either the whole surface was uniformly covered by varying amounts of Au or only selected areas were prepared in this way. For the latter purpose a mask was installed between the sample and the evaporation source which contained differently shaped holes such as circles (diameter 3 mm), grids, rectangles (1 mm×3 mm) and small ovals (0.5 mm in the long axis).

III. RESULTS

A. Surface characterization

Calibration of the Au coverage on the Pt(110) surface was achieved by CO titration: After deposition of Au whose relative amount was determined by the quartz microbalance, the surface was exposed to 5 L CO at 300 K (1 L $=0.75\times10^{-6}$ mbar s). Subsequently recorded thermal desorption spectra (TDS) as reproduced in Fig. 1 showed a linear decrease of the amount of adsorbed CO with Au concentration while the maximum temperature and the peak shape remained unaffected. This indicates that the Au atoms just block adsorption sites for CO without noticeable influencing the electronic properties of neighboring Pt surface atoms. Since a full monolayer of Au is known to completely inhibit CO adsorption at room temperature[16] in this way a convenient possibility for determining the absolute concentration of Au atoms was available.

With the clean Pt(110) surface the topmost atomic layer is reconstructed into a 1×2 phase which can be transformed into the bulklike 1×1 phase by adsorption of CO. Removal of the CO by thermal desorption or by reaction with oxygen restores the original 1×2 structure. Quite analogous behavior was observed by means of low energy electron diffraction (LEED) with the Au covered surfaces. Up to about 0.1 ML of Au, the CO induced 1×2→1×1 transformation and its reversal by reactive interaction with oxygen were found to proceed with about the same rates as with bare Pt(110). Up to about 0.5 ML Au both structural transformations were still found to proceed, however, with continuously slower speed. A surface covered by a full monolayer of Au exhibited a streaky 1×2-LEED pattern which was not affected any more by exposure to either CO or O_2, since such a surface is completely inert.

The work functions of the clean Pt(110) and Au(110) surfaces are 5.49 and 5.37 eV, respectively.[19,20] Such a difference manifests itself readily in the relative brightness of the PEEM images. In fact, patches covered with just 0.05 ML of Au could already be distinguished from neighboring bare Pt areas. Adsorption of CO and even more of O on Pt(110) causes the work function to increase leading to corresponding darkening of the PEEM images. The progress of adsorption could hence be qualitatively followed by recording the variation of the (normalized) PEEM brightness with gas exposure. Figures 2(a) and 2(b) show data for CO and O on both bare Pt(110) and a surface covered by 0.05 ML of Au. With CO the data for both kinds of surfaces were practically identical, indicating that the sticking coefficient on Pt sites is not affected by the presence of Au. This is quite in contrast to the results for dissociative oxygen chemisorption which is appreciably retarded by small amounts of Au. These findings are in agreement with general experience and will be of relevance for the interpretation of some of the features of pattern formation.

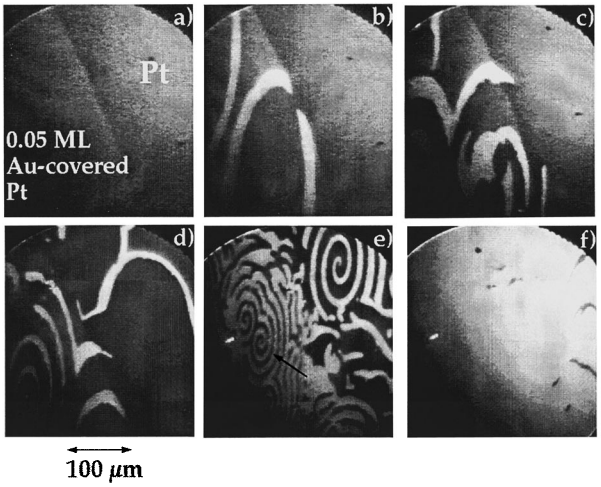

FIG. 3. PEEM images from a 0.05 ML Au-covered Pt(110) adjacent to a bare Pt area at $T=460$ K $p_{O_2}=4\times10^{-4}$ mbar for varying CO pressures: 1.0×10^{-5} mbar (a), 1.7×10^{-5} mbar (b); 1.9×10^{-5} mbar (c); 3.0×10^{-5} mbar (d); 4.6×10^{-5} mbar (e); 5.0×10^{-5} mbar (f).

B. Pattern formation on Pt(110) uniformly covered by Au

Figure 3 shows a sequence of PEEM images of a bare Pt(110) surface adjacent to an area which is covered by 0.05 ML of Au. The images were recorded at constant temperature and O_2 partial pressure and with varying CO pressures. At the lowest p_{CO} [Fig. 3(a)] both areas are predominantly covered by O_{ad}. Upon increasing p_{CO} to 1.7×10^{-5} mbar on the Au-covered side brighter patches develop reflecting the formation of CO_{ad} domains. Within these CO domains, again O_{ad} patches are nucleating and growing. This situation is characterizing the transition to a state of dynamic bistability.[9] The bare Pt area on the other hand, still remains in the O-covered state [Fig. 3(b)]. With further increase of p_{CO} to 1.9×10^{-5} mbar, CO fronts begin to form on the bare Pt area as well, first nucleating by diffusion across the boundary [Fig. 3(c)]. At even higher $p_{CO}=3\times10^{-5}$ mbar, CO spirals characteristic for the excitable state form on the Au-covered region, while on the bare Pt area propagating concentration fronts still prevail [Fig. 3(d)]. For $p_{CO}>4.6\times10^{-5}$ mbar, spiral patterns are discernible on both types of surfaces [Fig. 3(e)], however, the overall CO coverage on the Au-covered region exceeds that on the bare Pt surface. For this reason the spirals on the Au-covered part are dark (=oxygen) while they appear grey on the Pt area (=carbon monoxide). The front velocities at 460 K on the Au-covered part and on the bare Pt surface were 2.2 and 2.8 μm/s, respectively. The spiral wave on the Au-covered domain indicated by the black arrow in Fig. 3(e) has wavelengths of 18 ± 1 and 8 ± 1 μm in the [110] and [001] direction, respectively. The spiral on the bare Pt area, on the other hand, has wavelengths of 32 ± 1 and 15 ± 1 μm in the [110] and [001] directions, respectively. The ratios of the wavelengths in these two directions are 2.2 ± 0.2 and 2.1 ± 0.2 for the Au-covered and the bare Pt domains. The elliptical shape of the spiral waves both on the Au-covered region and on the unmodified Pt region is caused by an anisotropy in the diffusion coefficient of CO as described in Ref. 19. The similar ratios of the wavelengths show that the anisotropy of the CO diffusion is essentially unaffected by the presence of a submonolayer of Au. However, both the wavelength of the spirals as well as the front speed decrease in the presence of Au atoms. Finally, at $p_{CO}=5.0\times10^{-5}$ mbar, the Au domain is fully covered with CO while small oxygen waves still travel over the bare Pt region [Fig. 3(f)].

The qualitative features of the observed patterns are summarized in the phase diagrams of Fig. 4 at a fixed $p_{O_2}=4\times10^{-4}$ mbar as a function of temperature T and CO partial pressure (p_{CO}) for three different kinds of surfaces. The data for bare Pt(110) were taken from Ref. 10. As can be seen, for a given temperature the critical p_{CO} for transition from the monostable, O-covered state into the bistable or excitable regime, respectively, decreases with increasing Au coverage. The same holds for the transition from the excitable into the monostable, CO-covered state. In addition, the p_{CO} range over which patterns characteristic for the excitable state are formed, becomes narrower with increasing Au concentration.

With a surface covered by 0.3 ML of Au, pattern formation was no longer observed over the parameter range underlying Fig. 4. Oxygen and carbon monoxide adsorption was still possible, but upon increasing p_{CO} a direct transition

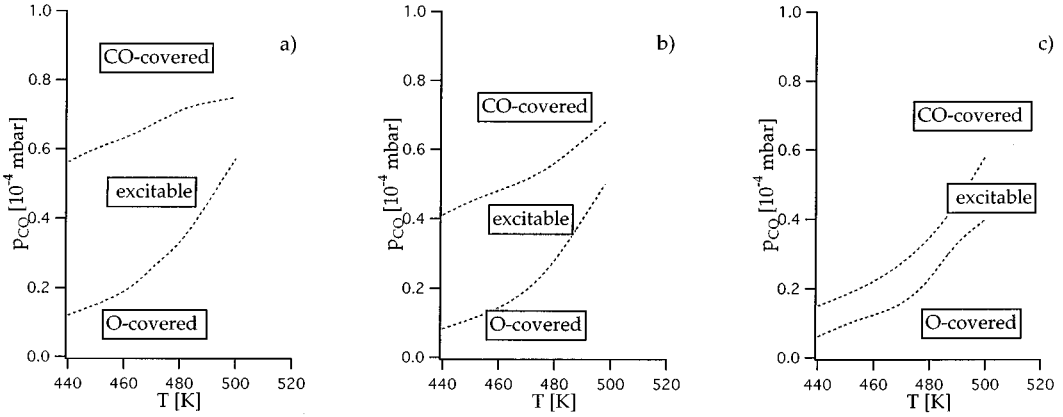

FIG. 4. Phase diagram marking the conditions for monostable O- and CO-covered regimens, respectively, and for bistability, and excitability, respectively as a function of T and p_{CO} fixed $p_{O_2}=4\times10^{-4}$ mbar. (a) Bare Pt(110); (b) surface covered by 0.05 ML Au; (c) 0.1 ML Au.

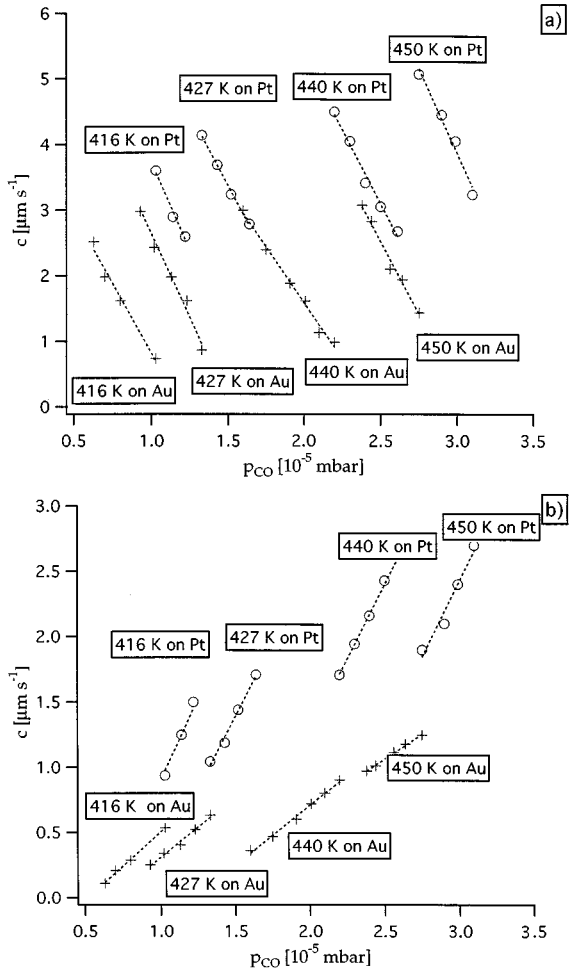

FIG. 5. Propagation speeds for O (a) and CO (b) fronts on bare and 0.05 ML Au-covered Pt(110) as a function of p_{CO} at constant $p_{O_2}=4\times10^{-4}$ mbar and different temperatures for conditions of dynamic bistability.

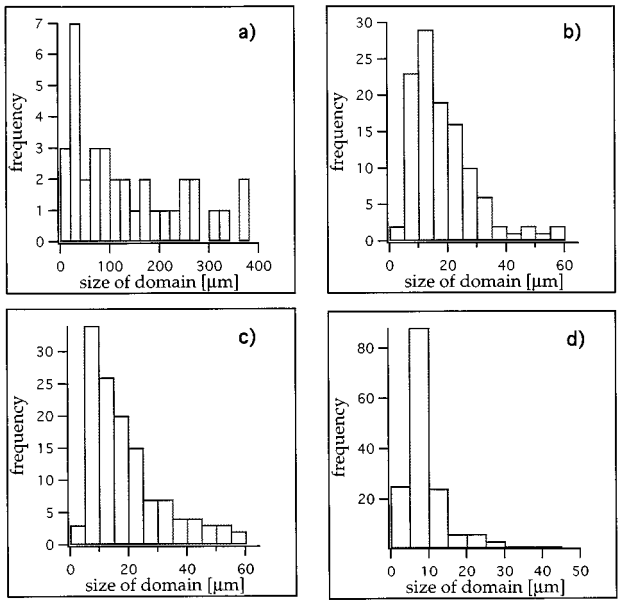

FIG. 6. Distribution of domain sizes for different surfaces. (a) bare Pt, (b) 0.05 ML Au, (c) 0.1 ML Au, (d) 0.2 ML Au. $T=450$ K, $p_{O_2}=4\times10^{-4}$ mbar. The CO pressures were adjusted to conditions close to the onset of dynamic bistability: 1.3×10^{-5} mbar (a), 1.1×10^{-5} mbar (b), 1.0×10^{-5} mbar (c), 0.8×10^{-5} mbar (d).

from the O-covered to the CO-covered state occurred.

As already mentioned, the presence of Au atoms causes a decrease of the front propagation velocity. Figure 5 summarizes the results of quantitative determinations of the velocities for O fronts [Fig. 5(a)] and CO fronts [Fig. 5(b)] within the regime of dynamic bistability along the [110] direction for both a bare Pt surface and for a sample covered by 0.05 ML of Au. For the same control parameters the velocity of the latter is generally considerably smaller (by up to a factor of about 4).

A detailed analysis of the density of nucleation centers and maximum size of CO domains within the bistable regime revealed that the presence of Au increased the former, but decreased the latter. On the bare Pt surface CO domains may grow up to diameters of about 100 μm. In contrast these are smaller, but more frequent, on the Au covered surface. Figure 6 shows histograms of the size distributions of CO domains for various types of surfaces for conditions close to the transition from the O-covered monostable into the bistable regime. The average domain size decreased from 140 μm for bare Pt(110) to 11 μm for the surface covered by 0.2 ML of Au. Obviously, already small Au concentrations cause a pronounced decreased of the typical domain sizes. On the other hand, the density of nucleation centers continuously increases as can be seen from the plot of Fig. 7.

Similar trends are observed within the regime of spiral waves. As became already evident from Fig. 3, the presence of Au causes a decrease of the wavelength λ as well as of the width of oxygen spiral arms. λ is correlated with the front propagation velocity c and with the rotation period of the spiral through $\lambda=\tau\cdot c$. Figure 8 shows the distributions of c, τ relations for both a bare and an Au covered Pt(110) surface for a fixed set of control parameters. The rotation periods were similarly distributed for both samples and were most frequently in the range between about 7 and 15 s. The generally smaller propagation velocities on the Au covered surfaces reflect the smaller wavelengths encountered there. Within the framework of a theory using an artificial core concept,[20,21] the rotation period τ is related to the core diameter R_0 and the front velocity c approximately by

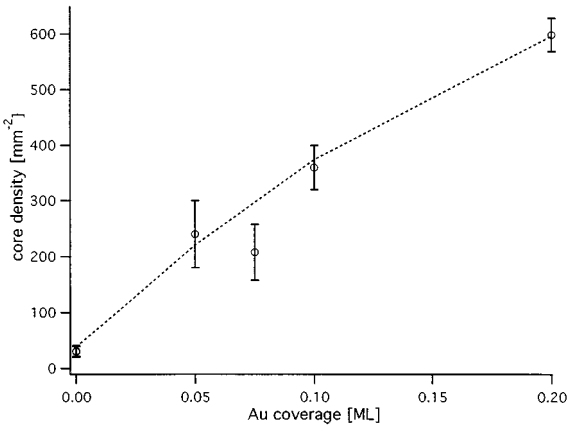

FIG. 7. Variation of the density of nucleation centers with Au coverage.

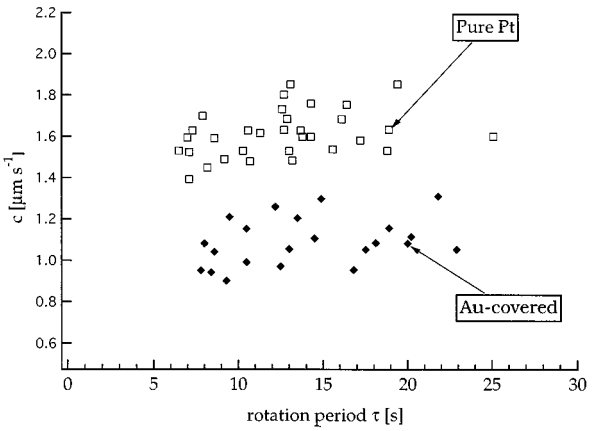

FIG. 8. Correlations between propagation velocity c along the $[1\bar{1}0]$ direction and rotation period τ for spiral waves on bare Pt(110) (open squares) and on a surface containing 0.05 ML Au (filled squares). $T=450$ K, $p_{O_2}=4\times10^{-4}$ mbar, $p_{CO}=4.2\times10^{-5}$ mbar.

$$\tau \approx \frac{2\pi R_0}{c}. \tag{1}$$

Since c is generally smaller on the Au-covered surface, for a given τ the core size also has to be correspondingly smaller.

As the temperature decreases or the Au coverage increases, the spiral waves become more and more distorted and eventually turn into turbulent patterns. This is demonstrated by Fig. 9 showing patterns from a 0.1 ML Au–Pt(110) surface recorded in a time interval of 10 s [Figs. 9(a) and 9(b)] and the computer generated difference image [Fig. 9(c)]. Some of the open ends of the oxygen waves tend to curl, but there is no full development of spirals. In Fig. 9(c) bright regions reflect the motion of oxygen fronts which appear as smooth lines followed by numerous small patches which are due to nucleation and growth of small CO domains. Thus oxygen domains are no longer converted by propagation of continuous CO fronts, but rather by frequent nucleation of CO domains inside the O domains.

This effect becomes even more pronounced if the CO pressure is further increased, such as from 6.3×10^{-6} to 6.6×10^{-6} mbar when going from Fig. 9 to Fig. 10. The latter

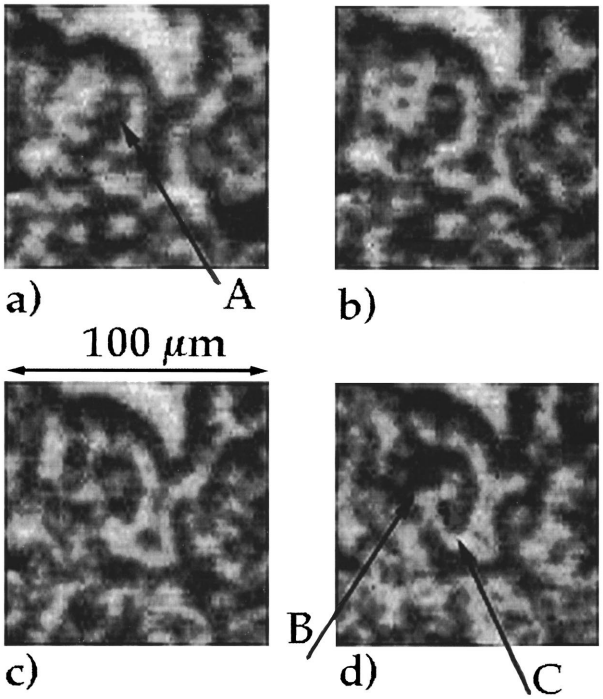

FIG. 10. PEEM images illustrating spiral break up on a Pt surface with 0.1 ML Au. $T=413$ K, $p_{O_2}=4\times10^{-4}$ mbar, $p_{CO}=6.6\times10^{-6}$ mbar. For explanation see the text.

figure shows a sequence of four magnified images recorded at time intervals of 10 s. As demonstrated by the arrow A in Fig. 10(a) nucleation of a CO domain is initiated inside the oxygen wave. It grows [Fig. 10(b)] and eventually breaks up the O wave [Fig. 10(c)]. The broken end then in turn starts to curl and transforms into a new spiral tip as shown by arrows B and C in Fig. 10(d). Events of this type are dominating the patterns formed under these control parameters applied.

At even higher CO pressure (6.8×10^{-6} mbar) the continuous breakup of spiral waves leads to the creation of numerous small fragments of oxygen waves. Their ends tend to curl, but before spirals can develop, they collide with other fronts and create again new fragments of oxygen waves so that the spiral waves collapse.

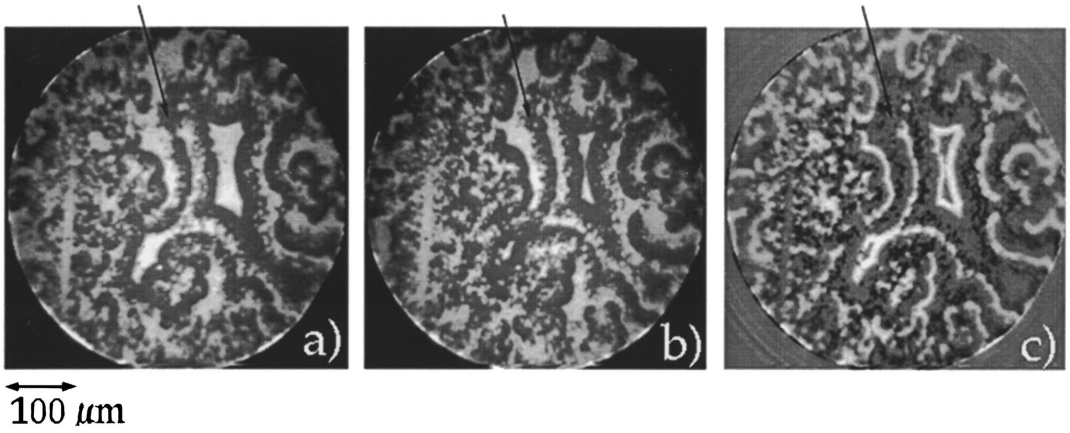

FIG. 9. PEEM images taken with an interval of 10 s [(a) and (b)] and difference image (c) from a Pt(110) surface with 0.1 ML Au showing the development of distorted spiral waves. $T=413$ K, $p_{O_2}=4\times10^{-4}$ mbar, $p_{CO}=6\times10^{-6}$ mbar.

TABLE I. MS: Monostable state (CO covered or O covered).

	State of Au-covered Pt	State of pure Pt
A	Excitable	O-MS
B	Excitable	O-MS, penetration
C	Excitable	Excitable
D	CO-MS, penetration	Excitable
E	CO-MS	Excitable

C. Effects at the boundaries

This section will describe a series of observations made in the border region between adjacent regions of bare Pt(110) and Au-covered surface. Figure 3(c) represented already an example for the kinds of effects which may occur, namely, the induction of fronts.

In classification of dynamical states described above in connection with Fig. 4 is summarized again in Table I and proceeds with increasing p_{CO} for fixed p_{O_2} and T. In state A the bare Pt surface is still in the O-covered, monostable state, while the Au-covered region is already bistable. CO-waves are created on this part of the sample, but they cannot cross the border to the bare Pt surface as reflected by the sequence of images in Fig. 11: A CO wave created inside the Au-covered region propagates towards the boundary [Figs. 11(a) and 11(b)] where it stops [Fig. 11(c)] and eventually breaks up and is annihilated [Fig. 11(d)].

At slightly higher CO pressure the system is in state B. The Pt part is still in the monostable O regime, but CO fronts propagating from the Au region may now cross the boundary [Fig. 12(a)]. In this case the CO wave moves with a velocity of 0.3 μm/s on the bare Pt. However, the consecutive O wave is much faster (0.95 μm/s) and thus rapidly extinguishes the CO wave [Figs. 12(b)–12(d)]. For given p_{O_2}, T the probability of a CO wave to cross the boundary increases with CO pressure rapidly beyond a critical threshold as shown in Fig. 13. This threshold is still markedly below the critical value for the nucleation and growth of CO waves inside the bare Pt area. The lifetime of such a CO wave on the Pt surface depends also on its size: Larger waves survive for longer times than smaller ones. This is reflected by the sequence of images shown in Fig. 14. While small CO waves as marked by arrows in Figs. 14(a), 14(b), and 14(g) may even not cross the border, the extended CO wave propagates far into the Pt region and survives there for more than 30 s.

In state C both phases are excitable and waves may readily pass the border in both directions. An example is shown in Fig. 15, where an O spiral with its core on the Au-covered part emits waves into the bare Pt area, where their width increases considerably. The speed along the [110] direction increases from 0.8 ± 0.2 to 1.3 ± 0.2 μm/s. The

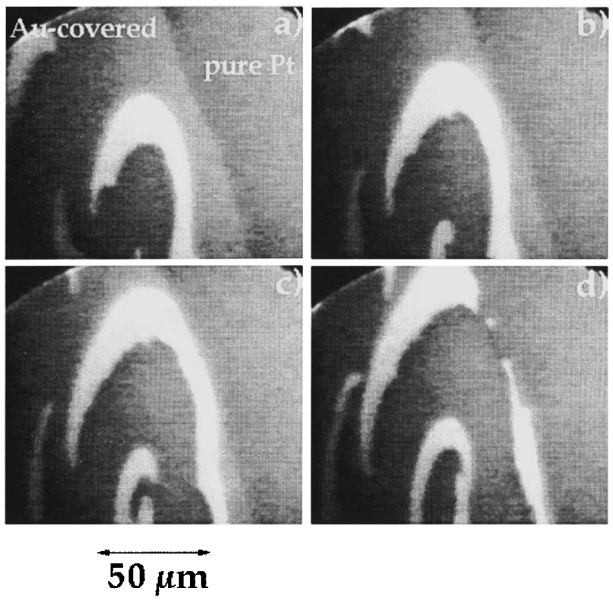

FIG. 11. PEEM images from a CO wave propagation near the boundary between a 0.05 ML Au covered and a bare Pt(110) surface. Both areas are predominantly covered by oxygen (dark regions). Time intervals 4 s. $T=480$ K, $p_{O_2}=4\times10^{-4}$ mbar, $p_{CO}=2.3\times10^{-5}$ mbar.

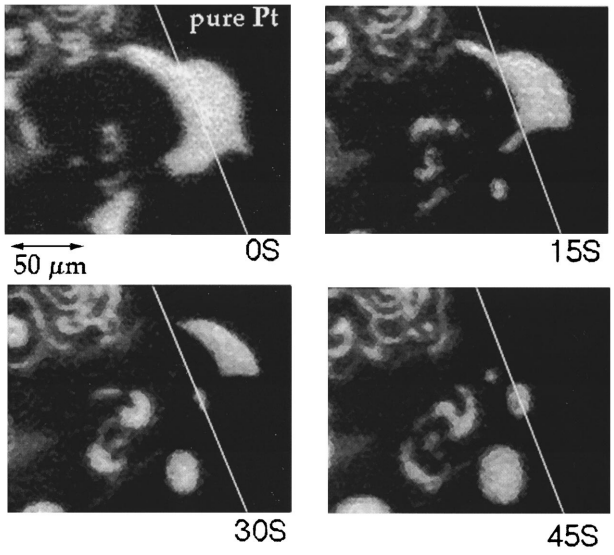

FIG. 12. PEEM images of a CO front crossing the border. Time intervals 15 s. $T=450$ K, $p_{O_2}=4\times10^{-4}$ mbar, $p_{CO}=1.4\times10^{-5}$ mbar.

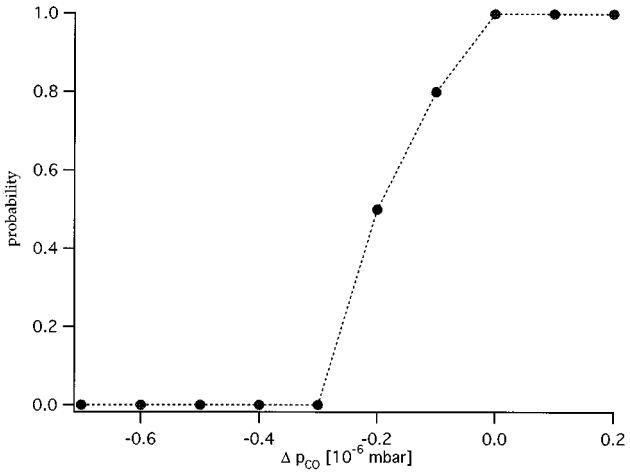

FIG. 13. Dependence of the probability for CO waves to cross the border between a 0.05 ML Au covered and a bare Pt surface as a function of p_{CO} for fixed $T=480$ K, $p_{O_2}=4\times10^{-4}$ mbar.

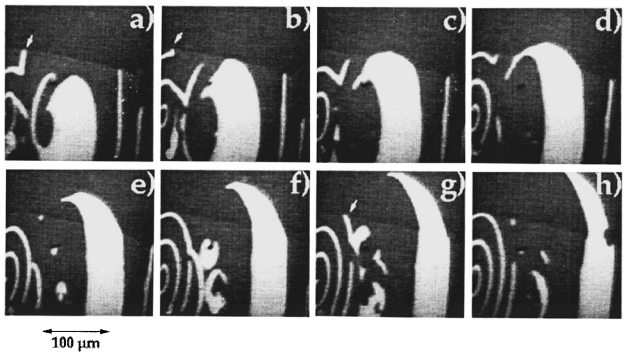

FIG. 14. Propagation and eventual extinction of CO waves in the bare Pt region after nucleation on the Au covered part of the surface. Time intervals 8 s. $T=480$ K, $p_{O_2}=4\times10^{-4}$ mbar, $p_{CO}=2.8\times10^{-5}$ mbar.

wavelength of the spirals on the bare Pt area is larger than on the Au-covered surface, in accordance with the findings described in Sec. III B.

Figure 16(a) shows another example in which the core of a spiral wave is located just on the border as indicated by an arrow. The tip is moving in and out of the Au-covered region with a rotation period of 18 s. The preferred creation of spirals at the border might be due to the higher density of defect sites acting as cores. More generally, any discontinuity of kinetic parameters may play such a role as also concluded in recent theoretical work on the formation of spiral waves in nonuniform systems.[22–24]

In Fig. 17, an O pulse travels with a velocity of 1.9 ± 0.2 μm/s through a Pt channel surrounded by a 0.05 ML Au-covered surface. Under these conditions we are in state *D* where the Au region is monostable and predominantly covered by CO, while the Pt surface is still excitable. The oxygen front is almost flat and perpendicular to the walls. Its ends ''leak'' into the Au-covered region by up to 40 μm until they are annihilated. The propagation velocity is thereby reduced to 1.4 ± 0.2 μm/s and the wave front forms an angle of $51°\pm6°$ with the border. The ratio of velocities in the two media is 1.36 ± 0.25 which is equal to $\sin\alpha_1/\sin\alpha_2=1.3\pm0.1$, where α_1 and α_2 are the angles of the wave fronts with the boundary.

This result is a manifestation of the phenomenon of refraction which is ubiquitous in wave propagation across a boundary and known as Snellius' law, $\sin\alpha_1/\sin\alpha_2=c_1/c_2$,

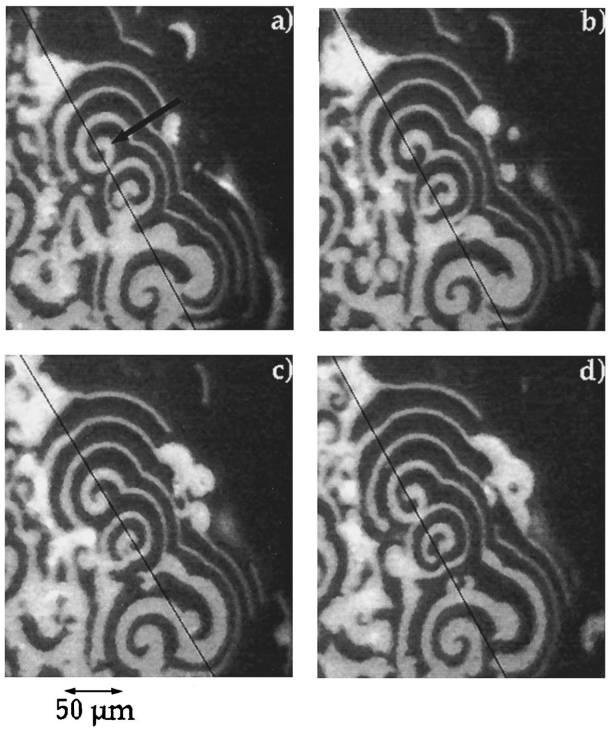

FIG. 16. PEEM images form spirals pinned to the boundary (black line) between Au covered and bare Pt surface. Time interval 8 s. $T=500$ K, $p_{O_2}=4\times10^{-4}$ mbar, $p_{CO}=4.1\times10^{-5}$ mbar.

where c_1 and c_2 are the propagation velocities in the two media. Zhabotinsky *et al.*[25] reported for the first time on the refraction of chemical waves in the BZ reaction obeying Snellius' law. Another example with the present system is demonstrated by Fig. 18, where an oxygen pulse propagates on the bare Pt surface with a velocity of 4.2 ± 0.2 μm/s and hits the border under an angle of $50°\pm3°$. On the Au-covered side the velocity decreases to 2.4 ± 0.2 μm/s, and the propagation direction changes to $69°\pm3°$ with respect to the border line. In this case is the ratio $c_1/c_2=1.75\pm0.2$ while for $\sin\alpha_1/\sin\alpha_2=1.8\pm0.2$ results, again confirming Snellius' law. With the present system, analysis of this effect could only be performed with small O pulses because of the otherwise high density of chemical waves. Reflection, as reported for the BZ reaction,[25] was not observed in the present context, however, was manifest with the same reaction oc-

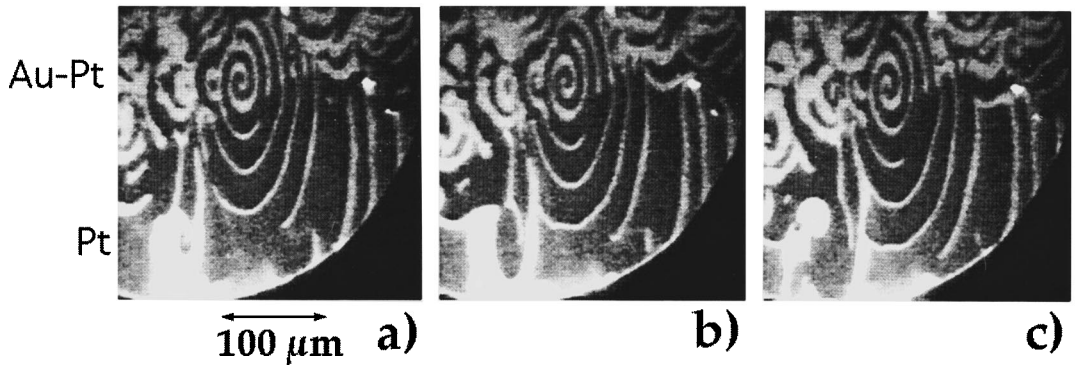

FIG. 15. Periodic wave trains originating from a spiral centered on the Au-covered part. $T=480$ K, $p_{O_2}=4\times120^{-4}$ mbar, $p_{CO}=4.8\times10^{-5}$ mbar.

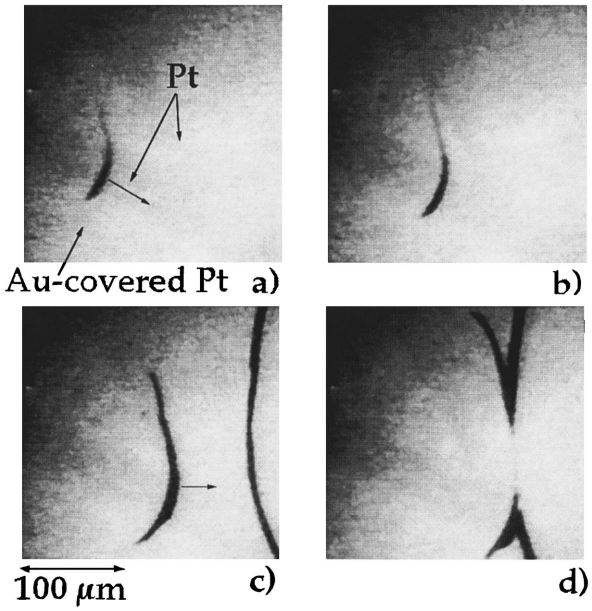

FIG. 17. Oxygen pulses traveling along a Pt channel surrounded by 0.05 ML Au-covered surface. Time intervals 20 s. $T=480$ K, $p_{O_2}=4\times10^{-4}$ mbar, $p_{CO}=5.3\times10^{-5}$ mbar.

curring on a Pt(100) surface partially covered by Au.[26]

For completeness it is added that finally in state *E* the Au surface is largely covered by CO and waves created on the Pt side may no longer cross the border, in analogy to the situation encountered in state *A*.

IV. DISCUSSION

The catalytic oxidation of CO on platinum surfaces proceeds through recombination between chemisorbed CO molecules and O atoms to CO_2 which is immediately released into the gas phase. With Pt(110) a reversible surface structural transformation ($1\times1\rightleftarrows1\times2$), driven by the CO coverage has, in addition, to be taken into account. The adsorption probability (sticking coefficient) for O_2 is, on the other hand, higher on the 1×1 than on the 1×2 phase which effect is responsible for the occurrence of kinetic instabilities for certain ranges of control parameters p_{CO}, p_{O_2}, and T. Based on knowledge about the individual reaction steps involved, a kinetic model was developed[11] which was extended into a set of coupled partial differential equations by inclusion of diffusion of adsorbed CO as the most mobile surface species[12–14]

$$\frac{\partial u}{\partial t}=k_u s_u p_{CO}[1-u^3]-k_2 u-k_3 uv+D\nabla^2 u,$$

$$\frac{\partial v}{\partial t}=k_v p_{O_2}[s_{v1}w+s_{v2}(1-w)][1-u-v]^2-k_3 uv, \quad (2)$$

$$\frac{\partial w}{\partial t}=k_5[f(u)-w].$$

Here, u and v are the (normalized) coverages of adsorbed CO and O, respectively, and w the fraction of the surface areas being present as 1×1 phase. $k_u p_{CO}$ and $k_v p_{O_2}$ are the rates of impingement of CO and O_2, respectively, from the gas phase onto the surface and s_u and s_v the associated sticking coefficients at zero coverage. s_u is equal (≈1) on the 1×1 and 1×2 phase, while s_v is larger on the 1×1 than on the 1×2 surface, viz. $s_{v1}=0.6$ and $s_{v2}=0.4$. D is the diffusion coefficient for adsorbed CO, and $f(u)$ is the equilibrium value for w at a given CO coverage for which the experimental data are approximated by a smooth polynomial function.

Based on this model, the effects of Au atoms on the pattern formation may now be qualitatively discussed. Thermal desorption experiments had demonstrated that the energetics of CO adsorption are not noticeably altered, but that the Au atoms act primarily as inert site blockers. It can hence be assumed that the rate coefficients on the Pt sites remain essentially unaffected. This conclusion holds also for the $1\times2\rightarrow1\times1$ structural transformation, whose rate constant (k_5) is only altered for higher Au coverages, $\theta_{Au}>0.3$.

The effect of gold is twofold.

(i) The Au atoms block adsorption sites for oxygen and CO adsorption. To a first approximation their influence on the rate of adsorption can be considered to be similar as that of the other adsorbates. That means that terms in Eq. (2) are altered as

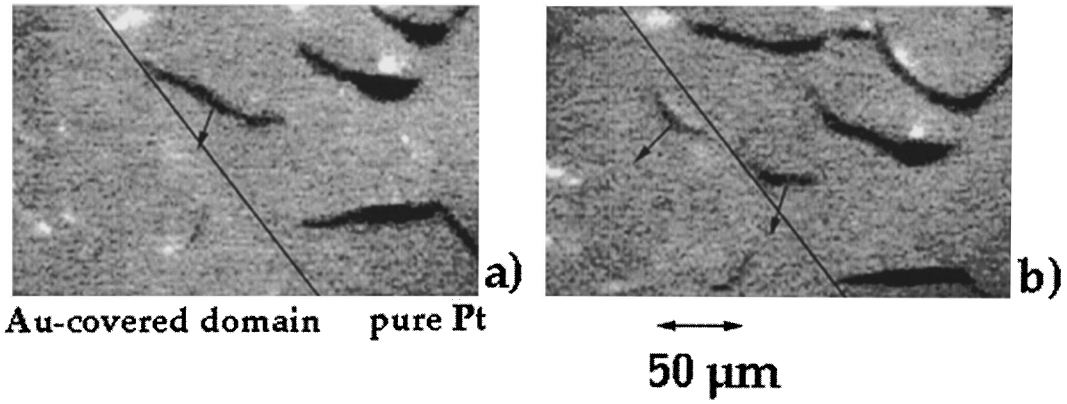

FIG. 18. Oxygen pulse traveling from the bare Pt into the Au-covered domain. Arrows indicate the directions of propagation. Time interval 8 s. $T=500$ K, $p_{O_2}=4\times10^{-4}$ mbar, $p_{CO}=6.6\times10^{-5}$ mbar.

$$[1-u^3]\rightarrow[1-(u+\theta_{\mathrm{Au}})^3],$$
$$[1-u-v]^2\rightarrow[1-u-v-\theta_{\mathrm{Au}}]^2. \tag{3}$$

In this way the different influence of Au coverage on CO and O adsorption as demonstrated by the experimental data for Fig. 2 is properly taken into account.

(ii) Since the adsorption energy of CO is much smaller on Au than on Pt, gold atoms act as obstacles for migrating CO molecules and will decrease the diffusion coefficient, i.e., to a first approximation

$$D=D_0(1-\theta_{\mathrm{Au}}). \tag{4}$$

These plausible assumptions based on experimental evidence enable qualitative rationalization of the presented findings on pattern formation.

(i) The transition with increasing p_{CO} from the monostable, primarily O-covered state to the bistable and excitable regime is governed by the balance between O and CO coverage. Since dissociative oxygen chemisorption is more affected by the presence of foreign atoms than CO adsorption [cf. Fig. 2 as modeled by Eqs. (3)] the critical CO pressure for this transition will be shifted to lower values with increasing θ_{Au}, in agreement with the experimental findings as summarized in Fig. 4. In a similar way, the sensitive suppression of oxygen adsorption by Au atoms favors at higher coverages CO adsorption even more, so that the shift of the transition from the excitable to the monostable, CO-covered regime occurs at still lower CO pressures. This causes a narrowing of the p_{CO} range over which the system is excitable which is again in agreement with the experimental observation reflected by Fig. 4.

(ii) The decrease of the wave propagation speed c as summarized in Fig. 5 can be traced back to the reduction of the effective diffusion coefficient for adsorbed CO. c is generally determined by the diffusion coefficient and effective first-order rate constant,[1,27,28] viz.

$$c=\sqrt{k_{\mathrm{eff}}\cdot D}. \tag{5}$$

The temporal and spatial coordinates in Eqs. (2) may be scaled to dimensionless variables $\hat{t}$ and $\hat{r}$ through the following transformations:[14]

$$\hat{t}=k_5 t,$$
$$\hat{r}=(k_5/D)^{1/2}\cdot r. \tag{6}$$

k_5 (the rate constant for the $1\times2\rightarrow1\times1$ transformation) can be regarded as independent of θ_{Au} as outlined above, while D is affected as formulated by Eq. (4). As a consequence, the presence of Au will reduce the actual length r for any given solution at a fixed $\hat{r}$ through the decrease of D. As a consequence the wavelength of the spiral patterns and any other characteristic lengths will be reduced by the presence of Au atoms, in agreement, e.g., with the experimental data summarized in Fig. 6. Because of the constancy of k_5, the time scale will, on the other hand, not be noticeably influenced. This is, for example, in agreement with the minimum spiral rotation period which was found to be about 7 s, independent of the Au coverage.

(iii) The presence of Au atoms increases the density of nucleation centers for spirals (see Fig. 7) which eventually leads to the formation of turbulent patterns. The distribution of these Au atoms is expected to be random *on atomic scale leading to uniformity on the mesoscopic scale (>1 μm)* and hence cannot be the direct origin for this effect, since these inhomogeneities are present on a scale much smaller than the minimum size of the nucleation centers. In fact, a more subtle effect is coming into play:

The velocity of propagation of a chemical wave c depends on the local radius of curvature R of its nucleation center as[1]

$$c=c_{\mathrm{pl}}-D/R, \tag{7}$$

where c_{pl} is the velocity of the corresponding plane wave. Defects can only trigger fronts if $c>0$ or if $D/R<c_{\mathrm{pl}}$. Thus there exists a minimum defect radius $R_{\mathrm{crit}}=D/c_{\mathrm{pl}}$. In previous work with bare Pt(110), R_{crit} for the smallest nucleation defects was found to be about 2 μm.[9] If the Au atoms would agglomerate to islands of comparable size and thus create new nucleation centers, these would clearly be discernible in the PEEM images which is not the case. However, since c_{pl} is proportional to $D^{1/2}$ also $R_{\mathrm{crit}}\propto D^{1/2}$ and hence decreases with the concentration of Au atoms. As a consequence, defects which would be too small to initiate the growth of waves on the bare Pt(110) surface may now act as nucleation centers and therefore their overall density increases.

Above about 0.1 ML of Au the density of stable cores becomes so high that the spiral arms break up so that eventually a transition to turbulent states takes place. Similar phenomena were already observed with the BZ reaction,[29,30] while theoretical calculations demonstrated the possibility for a transition to turbulence via breakup of spirals.[31]

(iv) Modification of the wave propagation properties by alteration of the kinetic parameters is also responsible for the phenomena observed at the boundaries of surface regions with different composition. Refraction and the validity of Snellius' law is a general effect of propagating waves as was also confirmed with the present system. Propagation into a region which is no longer excitable leads not to an abrupt extinction of the wave but to its survival over a length which depends on how far away the control parameters in the monostable phase are from transition into the excitable regime. Quite generally, the existence of nonuniformities or gradients in kinetic parameters and concentrations was found to affect spatiotemporal pattern formation in different systems.[32–35] Related effects had previously been reported for the catalytic CO oxidation on a cylindrical Pt single crystal[36] where reaction fronts were found to move across differing crystallographic orientations. This phenomenon is generally even more pronounced with small metal particles as used in ''real'' catalysis exposing different adjacent crystal planes and as demonstrated recently with a fine Pt tip imaged by field ion microscopy (FIM).[37] If the adjacent medium is, however, catalytically completely inert, the wall becomes impermeable and novel effects such as wave splitting, etc., come into play, as recently exemplified with Pt surfaces onto which microstructures of inert TiO_2 overlayers had been deposited.[38]

V. CONCLUSIONS

On the mesoscopic length scale of spatio-temporal pattern formation (>1 μm) associated with catalytic CO oxidation on a Pt(110) surface, evaporated Au atoms cause spatially uniform modification of the kinetic parameters for the elementary reaction steps. As a consequence the parameter range for transition from monostable into excitable regimes is shifted. Reduction of the diffusion coefficient for adsorbed CO leads to a decrease of the wave propagation velocity as well as of the critical radius for nucleation of spirals. The latter effect is responsible for the occurrence of ''turbulent'' patterns. If patches with different composition (such as bare and Au-covered Pt) are adjacent, waves from the excitable region may penetrate into the monostable areas before they are extinguished, and typical wave phenomena such as refraction obeying Snellius' law are observed.

The experimental findings may be qualitatively rationalized in the framework of the set of partial differential equations mimicking the reaction mechanism and successfully describing previous observations on pattern formation on an uncovered Pt(110) surface.

[1] A. S. Mikhailov, *Foundations of Synergetics I*, 2nd ed. (Springer, Berlin, 1994).
[2] *Chemical Waves and Patterns*, edited by K. Showalter and R. Kapral (Kluwer, Amsterdam, 1995).
[3] R. Imbihl, Progr. Surf. Sci. **44**, 185 (1993).
[4] M. Eiswirth and G. Ertl, in Ref. 2, p. 447.
[5] G. Ertl, Science **254**, 1750 (1991).
[6] S. Jakubith, H. H. Rotermund, W. Engel, A. von Oertzen, and G. Ertl, Phys. Rev. Lett. **65**, 3013 (1990).
[7] H. H. Rotermund, S. Jakubith, A. von Oertzen, and G. Ertl, Phys. Rev. Lett. **66**, 3083 (1991).
[8] M. Bär, M. Eiswirth, H. H. Rotermund, and G. Ertl, Phys. Rev. Lett. **69**, 945 (1992).
[9] S. Nettesheim, A. von Oertzen, H. H. Rotermund, and G. Ertl, J. Chem. Phys. **98**, 9977 (1993).
[10] W. Engel, M. Kordesch, H. H. Rotermund, S. Kubala, and A. von Oertzen, Ultramicroscopy **36**, 148 (1991).
[11] K. Krischer, M. Eiswirth, and G. Ertl, J. Chem. Phys. **96**, 9161 (1992).
[12] M. Bär, C. Zülicke, M. Eiswirth, and G. Ertl, J. Chem. Phys. **96**, 8595 (1992).
[13] M. Falcke, M. Bär, H. Engel, and M. Eiswirth, J. Chem. Phys. **97**, 4555 (1992).
[14] M. Bär, N. Gottschalk, M. Eiswirth, and G. Ertl, J. Chem. Phys. **100**, 1202 (1994).
[15] J. W. A. Sachtler, M. A. van Hove, J. P. Biberian, and G. A. Somorjai, Surf. Sci. **110**, 19 (1981).
[16] P. W. Davies, M. A. Quinlan, and G. A. Somorjai, Surf. Sci. **121**, 290 (1982).
[17] K. Asakura, J. Lauterbach, H. H. Rotermund, and G. Ertl, Phys. Rev. B **50**, 8043 (1994).
[18] H. H. Rotermund, W. Engel, S. Jakubith, A. von Oertzen, and G. Ertl, Ultramicroscopy **36**, 164 (1991).
[19] A. von Oertzen, S. Nettesheim, and H. H. Rotermund, Surf. Sci. (in press, 1995).
[20] M. Bär, M. Falcke, and M. Eiswirth, Physica A **188**, 78 (1992).
[21] J. P. Keener and J. J. Tyson, Physica D **21**, 307 (1986).
[22] A. V. Panfilov and B. N. Vasiev, Physica D **49**, 107 (1991).
[23] A. Babloyantz and J. A. Sepulchre, Physica D **49**, 52 (1991).
[24] A. M. Pertsov, E. A. Ermakova, and E. E. Shnol, Physica D **44**, 178 (1990).
[25] A. M. Zhabotinsky, M. D. Eager, and I. R. Epstein, Phys. Rev. Lett. **71**, 1526 (1993).
[26] K. Asakura, J. Lauterbach, H. H. Rotermund, and G. Ertl (in preparation).
[27] R. Luther, Z. Elektrochem. **12**, 596 (1906).
[28] K. Showalter and J. J. Tyson, J. Chem. Educ. **64**, 742 (1987).
[29] K. I. Agladze, V. I. Krinsky, and A. M. Pertsov, Nature (London) **308**, 834 (1984).
[30] J. Maselko and K. Showalter, Physica D **49**, 21 (1991).
[31] M. Bär and M. Eiswirth, Phys. Rev. E **48**, R1635 (1993).
[32] H. Linde and C. Zirkel, Z. Phys. Chem. **174**, 145 (1991).
[33] L. Gil, K. Emilson, and G. L. Oppo, Phys. Rev. A **45**, R567 (1992).
[34] J. H. Block, M. Ehsasi, and V. Gorodetskii, Progr. Surf. Sci. **42**, 143 (1993).
[35] A. M. Zhabotinsky, S. C. Müller, and B. Hess, Chem. Phys. Lett. **172**, 445 (1990).
[36] M. Sander, R. Imbihl, and G. Ertl, J. Chem. Phys. **97**, 5193 (1992).
[37] V. Gorodetskii, J. Lauterbach, H. H. Rotermund, J. H. Block, and G. Ertl, Nature (London) **370**, 276 (1994).
[38] M. D. Graham, I. G. Kevrekidis, K. Asakura, J. Lauterbach, K. Krischer, H. H. Rotermund, and G. Ertl, Science **264**, 80 (1994).